Switching of anisotropy and phase diagram of the Heisenberg square-lattice $S = \frac{1}{2}$ antiferromagnet $Cu(pz)_2(ClO_4)_2$

K. Yu. Povarov,[1] A. I. Smirnov,[1,2] and C. P. Landee[3]
[1]*P. L. Kapitza Institute for Physical Problems, RAS, 119334 Moscow, Russia*
[2]*Moscow Institute for Physics and Technology, 141700 Dolgoprudny, Russia*
[3]*Department of Physics, Clark University, Worcester, Massachusetts 01610, USA*
(Received 15 March 2013; published 3 June 2013)

Experiments in the antiferromagnetic phase of a quasi-two-dimensional $S = 1/2$ quasi-square-lattice antiferromagnet $Cu(pz)_2(ClO_4)_2$ reveal a biaxial type of anisotropy, instead of the easy-plane one considered before. The weak in-plane anisotropy, found by means of electron spin-resonance spectroscopy and magnetization measurements, is about an order of magnitude weaker than the off-plane anisotropy. The weak in-plane anisotropy results in a spin-flop phase transition for the magnetic field aligned along the easy axis, and, thereby, in a bicritical point on the phase diagram. A remarkable feature of the weak in-plane anisotropy is the abrupt change of its sign at the spin-flop point. This anisotropy switching disappears at the tilting of the magnetic field to the easy axis by the angle of 10° within the plane. The nature of the abrupt anisotropy reversal remains unclear. The phase diagram is characterized by the increase of the ordering temperature T_N in the magnetic field used, except for a dip near the bicritical point.

DOI: 10.1103/PhysRevB.87.214402 PACS number(s): 75.40.Gb, 75.50.Ee, 76.50.+g

I. INTRODUCTION

The Heisenberg $S = 1/2$ antiferromagnet on a square lattice (HSLAF) is a popular model of low-dimensional magnetism.[1] An ideal HSLAF has no long-range order except at $T = 0$, where a Néel-type ground state with 40% reduction of the ordered spin component should be realized.[2] In a real *quasi*-two-dimensional (quasi-2D) antiferromagnet, a weak interlayer interaction is present, providing a Néel order at $T > 0$. An organometallic compound $Cu(pz)_2(ClO_4)_2$ (copper pyrazine perchlorate) has been considered as an example of quasi-2D HSLAF: copper ions carrying spin $S = 1/2$ are bridged together in slightly distorted square-lattice layers by pyrazine ($C_4H_4N_2$) rings, as shown in Fig. 1.

Copper pyrazine perchlorate crystallizes from a solution in the space group $C2/m$ at room temperature; however, at cooling, near 180 K, there is a phase transition to a structure which has the space group $C2/c$ (Ref. 3). In the low-temperature phase, parameters b and c of the monoclinic lattice are close to each other. The rectangles with sides b and c are approximately squares. Diagonals of these rectangles form a rhombic lattice, and these rhombuses are slightly distorted squares. The angle between the a and c axes differs only a little from 90°, thus the lattice may be represented as a weakly distorted tetragonal lattice. Magnetic ions Cu^{2+} ($S = 1/2$), placed at the corners of rhombuses, form layers in bc planes. The nearest-neighbor exchange paths are symmetrically equivalent and exactly identical. Therefore, the exchange network within the bc planes is equivalent to that of a square lattice. Due to ClO_4 complexes between the layers, they are well separated, as well as due to half of a period in-plane shift between layers. Because of this shift, a magnetic ion within a layer is equidistant from four ions in the adjacent layer; therefore, the interlayer coupling is canceled in the first order.[3]

Indeed, estimation of the interlayer effective exchange $J_\perp$ from values of $T_N = 4.25$ K and nearest-neighbor exchange $J = 18.1$ K by an empirical relation $J_\perp/J \sim \exp(-\frac{2.3J}{T_N})$, derived from quantum Monte Carlo simulation,[4] leads to a very small value of $J_\perp \simeq 9 \times 10^{-4} J$ (Ref. 5). The magnetic moment per Cu^{2+} ion in the two sublattice structures is only $0.47\mu_B$ at $T \to 0$ in the zero field, as detected by elastic neutron scattering.[6] This quantum spin reduction indicates a strong influence of quantum fluctuations on the ground state. From the observation of an increase of the ordered spin component in the external field, Tsyrulin *et al.*[6] conclude that the fluctuations are suppressed by the magnetic field. A related evidence of fluctuation suppression is the significant growth of T_N in the magnetic field, confirmed by neutron scattering and specific-heat measurements.[6] A gap of $E_0 \simeq 0.2$ meV in the spin-wave spectrum, detected by inelastic neutron scattering,[6,7] was ascribed to easy-plane (XY-type) anisotropy, keeping the spins within the bc plane. The observation of the minimum in susceptibility vs temperature dependence for a field directed perpendicular to the bc plane is consistent with quantum Monte Carlo (QMC) simulations,[8] which predict the minimum of the susceptibility for HSLAF with a small XY anisotropy.

We describe systematic investigations of $Cu(pz)_2(ClO_4)_2$ by means of multifrequency electron spin-resonance (ESR) spectroscopy and magnetization measurements for different orientations of the magnetic field. Our main result is the observation and measurement of a weak in-plane anisotropy. This weak anisotropy induces remarkable features of the phase diagram. These are (i) the spin-flop phase transition in a magnetic field applied along the easy axis, (ii) a bicritical point, and (iii) a dip in $T_N(H)$ dependence near the bicritical point. From the antiferromagnetic resonance spectrum, we also find that the weak in-plane anisotropy surprisingly changes its sign by a jump at the spin-flop point. Besides, this effect of abrupt anisotropy reversal arises as another phase transition at tilting of the magnetic field, at a critical angle between the magnetic field and the easy axis.

II. EXPERIMENT

Samples of $Cu(pz)_2(ClO_4)_2$ have been grown at Clark University as described in (Ref. 3). The lattice parameters of the

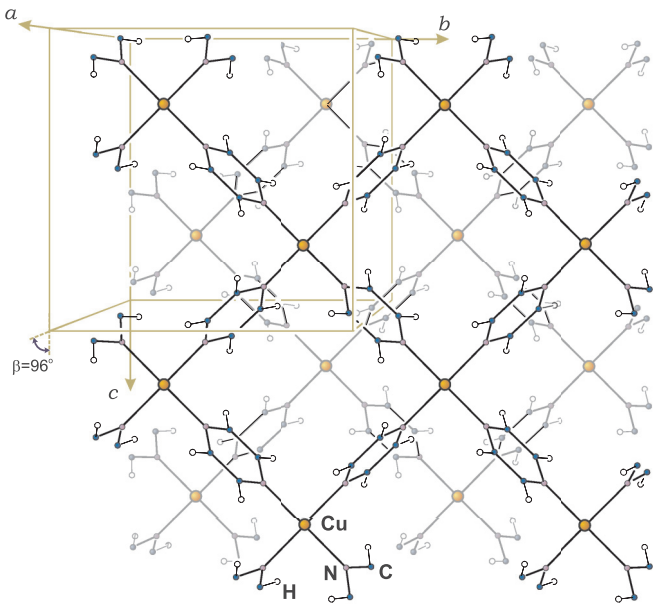

FIG. 1. (Color online) $Cu(pz)_2(ClO_4)_2$ structure. Two layers, each containing a square magnetic lattice, are displayed; ClO_4 complexes are not shown for clarity. Colors of ions and connecting lines in the lower layer are faded out. Crystallographic data are taken from Ref. 3.

monoclinic $C2/c$ lattice are $a = 14.072(5)$, $b = 9.786(3)$, and $c = 9.781(3)$ Å; $\beta = 96.458(4)^\circ$. Crystals are flat rectangular plaquettes colored blue, of the typical size of 2×2 mm^2; the plane of the square lattice (bc plane) coincides with the plane of the plaquette. The sides of the square crystal plaquettes are aligned at 45° to the b and c axes, coinciding with the directing lines of the magnetic square lattice; see a sketch on the margins of Fig. 4.

ESR experiments were performed at the Kapitza Institute, using a set of resonator spectrometric inserts in a ^{4}He pumping cryostat with a cryomagnet. The frequency range from 5 to 140 GHz was covered. A spectrometric insert for the 18–140 GHz range has a rotable sample holder, allowing one to change the orientation of the sample with respect to the magnetic field during the experiment. A small amount of diphenylpicrylhydrazyl (DPPH), a free-radical compound with $g = 2.00$, was used as a magnetic field label.[9]

Magnetization experiments were performed at the Department of Low Temperature Physics and Superconductivity of M. V. Lomonosov Moscow State University on the Quantum Design 9 Tesla PPMS machine equipped with a vibrating sample magnetometer (VSM) and at the Neutron Scattering and Magnetism Group in the Laboratory for Solid State Physics at ETH Zürich with the identical machine. The lowest available temperature was 1.8 K.

III. ESR DATA

A. Temperature evolution of ESR signal

The magnetic resonance signal in $Cu(pz)_2(ClO_4)_2$ at temperatures above $T_N = 4.2$ K corresponds to a typical exchange-narrowed paramagnetic resonance of Cu^{2+} ions with anisotropic g factor. The values of the g factor, obtained by high-temperature ($T \gtrsim 10$ K) ESR measurements, are $g_x = g_y = 2.05$ and $g_z = 2.28$. A narrow Lorentzian line, with a half-width of about 5×10^{-3} T, broadens with cooling and becomes unresolvable near T_N. Below T_N, the ESR response becomes strongly anisotropic. For $\mathbf{H} \parallel z$, a broad signal transforms into a single narrow line, shifted from the high-temperature position, while for $\mathbf{H} \parallel x, y$, two lines appear, as shown on the left panel of Fig. 2. The resonance half-width shows a clear critical dependence near the phase-transition temperature. The divergency in the line half-width together with the shift of the resonance position, as shown in Fig. 3, can be used as a marker of the phase transition, allowing us to extract T_N from the ESR data. The value of $T_N = 4.2 \pm 0.1$ K is in agreement with the results of the magnetization measurements, as shown on the phase diagram (Fig. 16).

B. Antiferromagnetic resonance

The anisotropy within the bc plane below T_N results in the angular dependence of the resonance field, as shown in

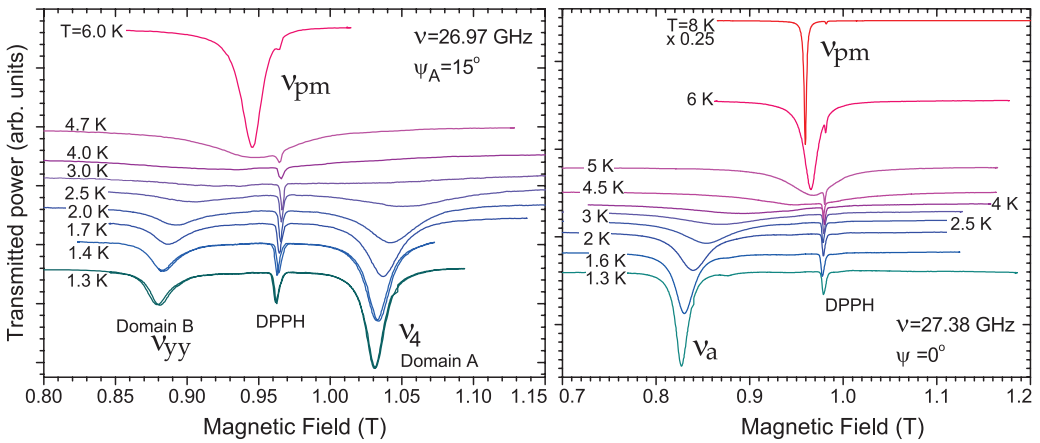

FIG. 2. (Color online) Left panel: Resonance line temperature evolution in a sample, containing two types of domains, when $\psi_A = 15^\circ$. Right panel: Resonance line temperature evolution in a single domain sample when $\psi = 0^\circ$. In both cases, $\xi = 0^\circ$, i.e., the field lies in the xy plane. The angles ψ and ξ are defined in Fig. 4. A scaling factor of 0.25 is applied to the 8 K line on the right panel.

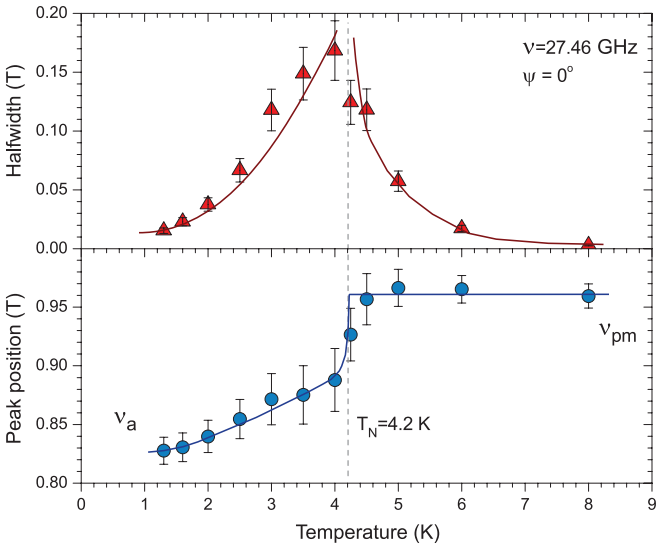

FIG. 3. (Color online) Changes of resonance field and linewidth through T_N in a single domain sample for $\mathbf{H} \parallel x$ at $\nu = 27.46$ GHz; corresponding set of ESR signals is shown in the right panel of Fig. 2. Lines are a guide to the eye.

Figs. 4 and 5. This reveals two kinds of resonances with the identical rosettelike angular dependencies, which are shifted for 90° in Fig. 4. The relation between the intensities of these two kinds of signals is different for different samples. This observation indicates a presence of two kinds of domains. The ratio of intensity of signals from two kinds of domains has the same value for zero-field cooling and field cooling of the sample in the field of 6 T, as well as at thermocycling through T_N. Therefore, we conclude that these domains are crystallographic domains for which b axes are rotated for 90 °. We denote domains with orthogonal b (c) axes as domain

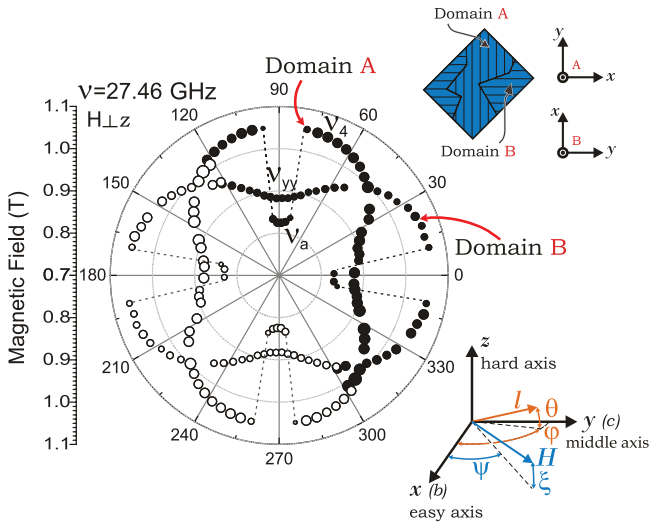

FIG. 4. (Color online) Polar plot of 27.46 GHz ESR field at rotating $Cu(pz)_2(ClO_4)_2$ sample in the bc plane; $T = 1.3$ K. Solid symbols correspond to actual experimental data, and open symbols are the repetition of solid symbols with the 180° period. Symbol size corresponds to resonance intensity. Dashed lines are a guide to the eye. A rough sketch of a two-domain sample and orientation of the x,y,z axes within domains is shown.

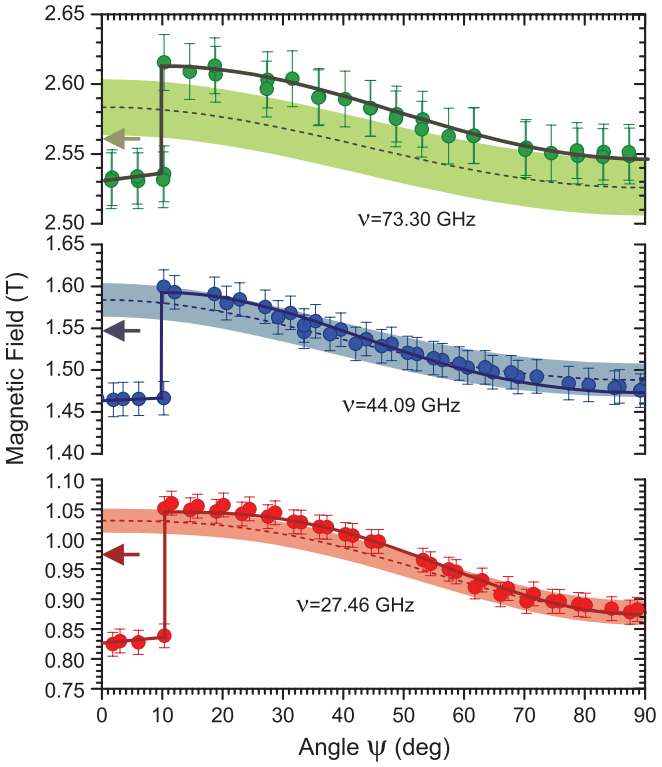

FIG. 5. (Color online) Summary of angular dependencies in the xy plane for a domain. Solid lines are a guide to the eye; dashed lines are the theoretical calculation (biaxial model) with a shaded region around it, marking a possible error due to the parameters uncertainty. Arrows indicate the field of paramagnetic resonance at the corresponding frequency.

A and domain B. One of the samples has the intensity for one rosette that is much stronger than for another one. For this approximately single-domain sample, the relation between the volumes of domains of different types may be evaluated, e.g., from the relation of intensities of ESR lines presented in Fig. 6, upper panel, between 0.82 and 0.88 T. Such an estimation gives the number of spins belonging to domain A, which is approximately 30 times greater than those of domain B. This sample remained approximately single domain at numerous cycles of cooling from the room temperature.

The rosettes shown in Fig. 4 demonstrate a smooth evolution of the resonance field with the angle in the whole angle range, except for the narrow range in the vicinity of the b direction. This direction was identified for the nearly single-domain sample by room-temperature x-ray diffraction. At the angle $\psi = 10°$, there is a steplike jump of the resonance field, shown in Figs. 4 and 5. Near the exact orientation of the external field along the b axis, i.e., when tilting ψ does not exceed 10°, the resonance field is shifted to a much lower field and this position cannot be extrapolated from the smooth angular dependence in the main part of the field range. Therefore, we denote the resonance observed at $|\psi| < 10°$ as anomalous mode ν_a. The redistribution of the intensity from the regular to the anomalous mode at a slow rotation of the field is shown in Fig. 6. One can see here that the transmission of the intensity between the two types of resonances has the character of a switching; it is performed within an interval

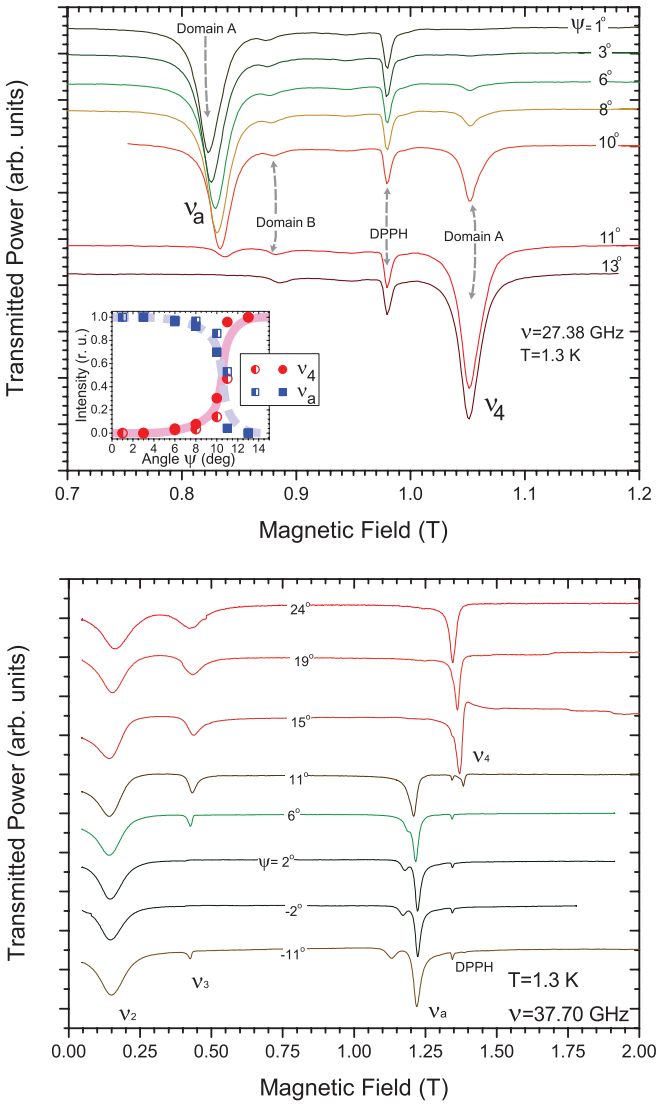

FIG. 6. (Color online) Evolution of the ESR line of a single-domain sample at the rotation of the magnetic field within the xy plane near the critical angle $\psi_c = 10°$, when regular mode ν_4 transforms to anomalous mode ν_a. Zero-field cooling from 15 K to $T = 1.3$ K was performed before each record. Upper panel: $\nu = 27.28$ GHz. Lower panel: $\nu = 37.7$ GHz. Inset: Angular dependences of the intensities of ESR modes ν_4 (red circles) and ν_a (blue squares). Each half-open symbol corresponds to a line recorded after zero-field cooling. Solid symbols present ESR lines recorded without thermocycling, with each rotation performed in a field 1.2 T. Thick lines are a guide to the eye.

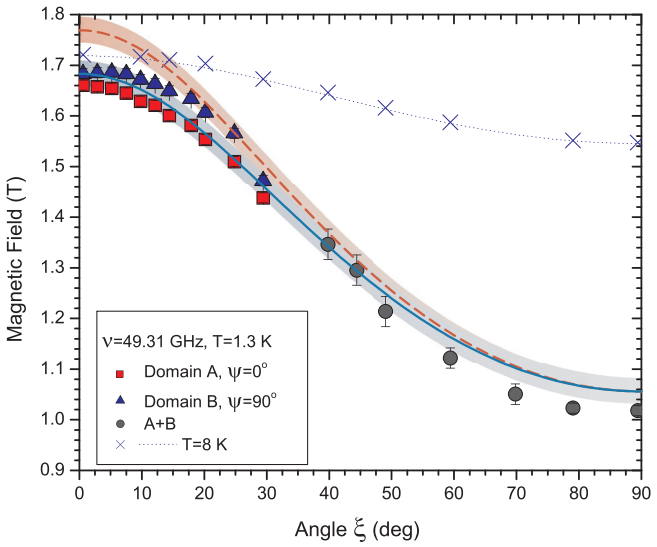

FIG. 7. (Color online) Angular dependence of the field of 49.31 GHz ESR in a two-domain sample of $Cu(pz)_2(ClO_4)_2$ at the temperature $T = 1.3$ K. Rotation is performed in the xz plane of the domain A. Triangles: domain A; squares: domain B; circles: signal of the whole sample when domains become indistinguishable; crosses: $T = 8$ K. Solid line presents the calculated low-temperature resonance field (biaxial model) for $\psi = 90°$; dashed line is for $\psi = 0$ and dotted line is theory for high-temperature paramagnetic resonance. The shaded region marks error boundaries of the model calculation (see text).

of about 1°, which may be a measure of the mosaic of the sample. Thus, a narrow phase transition at the angle variation is observed.

To check the dependence of this transition on magnetic and thermal history, we used the following four different regimes of generation of the state with anomalous magnetic resonance mode: (1) rotation of the sample from an angle $\psi > \psi_c$ to an angle $\psi < \psi_c$ in a field of 3 T at $T = 1.3$ K, (2) the same rotation in the zero field at $T = 1.3$ K, (3) the same rotation at $T > T_N$, $\mu_0 H = 3$ T, followed by cooling down to $T = 1.3$ K, and (4) rotation at $T > T_N$, $H = 0$, with magnetization at $T = 1.3$ K. All methods have resulted in identical ESR lines for the frequencies, listed in Fig. 5. Thus, no difference between the ordered states prepared by different field-cooling and zero-field-cooling procedures has been found.

Tilting the field within the xz plane conserves the anomalous mode, as shown in Fig. 7, at least in the range $|\xi| \lesssim 30°$, where the difference between the anomalous mode and an extrapolation for a regular mode may be detectable. The anomalous mode was observed only at $\mu_0 H > 0.4$ T. Below this field, the resonance positions at $\psi = 0°$ and $\psi = 15°$ are almost identical, as one can see on the upper and lower records of Fig. 8 and on the low-field part of frequency-field dependencies on the inset of Fig. 9. At the same time, at $\mu_0 H > 0.4$ T, there is a jumplike evolution of the resonance field and frequency in this range of angles.

Further, we measured ESR fields for a set of frequencies (see examples of records in Fig. 8) at three principal directions of the magnetic field and at a tilting angle $\psi = 15°$, as well as for two intermediate orientations in the bc plane. The corresponding frequency-field dependencies are presented in Figs. 9 and 10. From these data, we conclude that the spectrum of frequencies of the antiferromagnetic resonance has two energy gaps, approximately equal to 35 and 10 GHz, and two branches in a magnetic field. For the direction of the magnetic field near the b axis, there is a mode softening at approaching the field of 0.42 T from the zero-field side. At $\mu_0 H > 0.42$ T, we observe the softened mode in the angular range of the regular mode and the anomalous mode in the narrow angle range $|\psi| < 10°$. By changing the angle ψ across the critical value toward $\psi = 0$, the ESR frequency is transposed from the value below the paramagnetic resonance frequency,

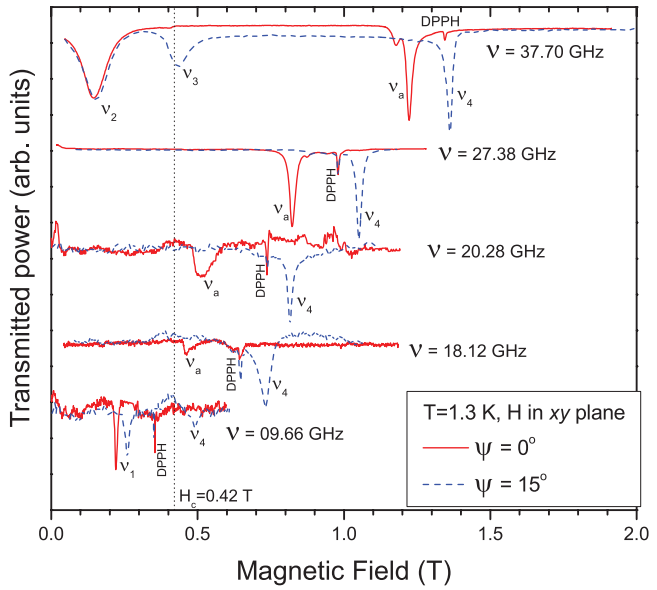

FIG. 8. (Color online) Collection of ESR lines at $T = 1.3$ K for fields along $\psi = 0^\circ$ (red solid) and $\psi = 15^\circ$ (blue dashed). Vertical dashed line denotes critical field $H_c = 0.42$ T at this temperature.

$g_x\mu_B\mu_0 H/2\pi\hbar$, to the value above it. This transposition is marked by an arrow on the inset of Fig. 9; it occurs by a jump at crossing the critical angle $\psi_c = 10^\circ$. This jump corresponds exactly to the jump of the resonance field, shown in Fig. 5.

We note here that the observed frequency-field dependencies for field orientation in the whole solid angle, except for the range of the anomalous mode, may be well described by the calculated frequencies of the two sublattice antiferromagnets with a biaxial anisotropy and the easy axis directed along b; see, e.g., Ref. 10. The calculated frequencies are given in Appendix A and presented in Figs. 9 and 10 by solid

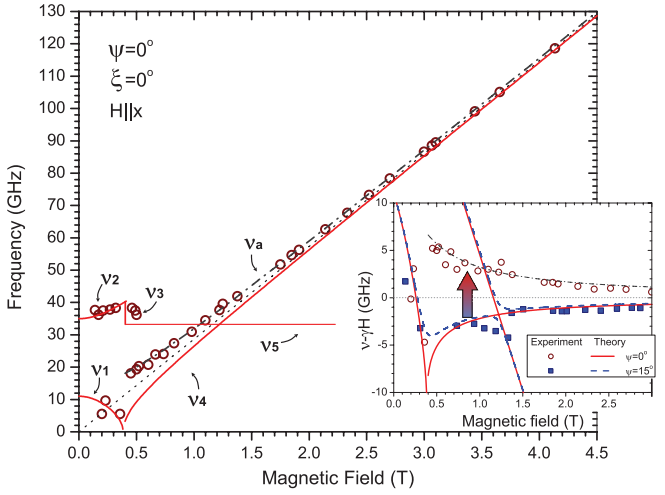

FIG. 9. (Color online) AFMR spectra at $T = 1.3$ K for the field along the easy axis. Solid line is the model calculation; dash-dotted line is the empirical formula (1). Inset: Shift from paramagnetic resonance frequency vs field for directions $\psi = 0^\circ$ (empty circles) and $\psi = 15^\circ$ (solid squares) in the xy plane. Solid and dashed lines are theoretical calculations corresponding to these cases. Dash-dotted line is the same as on main plot.

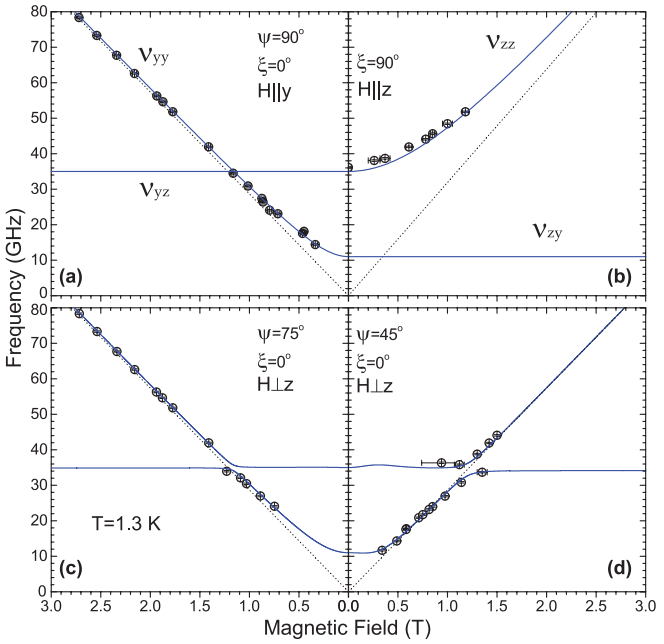

FIG. 10. (Color online) AFMR spectra for several field directions in the xy plane and along the z axis at $T = 1.3$ K. Solid lines are the calculation according to (B2) with $\Delta_y = 11$ GHz and $\Delta_z = 35$ GHz; dashed lines are paramagnetic resonance with $g_{xy} = 2.05$ and $g_z = 2.28$.

lines. The eight curves shown here and the calculated angular dependencies shown in Fig. 7 are parameterized only by two energy gaps and three g factors. The g factors g_x, g_y, and g_z are measured independently in the paramagnetic phase and are not fitting parameters. Below the critical field of 0.42 T, the frequencies in the whole solid angle range of the magnetic field directions are described with that model. In particular, a mode softening at $\mathbf{H} \parallel b$ indicates the spin-flop transition. By this observation, we can conclude that b is the easy-axis direction. For the anomalous mode, observed at $|\psi| < 10^\circ$, $|\xi| < 30^\circ$, $\mu_0 H > 0.42$ T, we use the empirical relation

$$\nu_a = \sqrt{\Delta_a^2 + \left(\frac{g_x\mu_B}{2\pi\hbar}\mu_0 H\right)^2}, \qquad (1)$$

with $\Delta_a = 14$ GHz at $T = 1.3$ K. This relation represents the observed frequency at the unexpected position above (and not below) the paramagnetic resonance frequency at $H > H_c$.

Thus, the ESR data reveal a weak magnetic anisotropy in the bc plane and a spin-flop transition, as well as the anomalous mode ν_a appearing in the narrow angular range of the field direction instead of a regular resonance of a biaxial antiferromagnet.

IV. MAGNETIZATION

A. Field along the easy axis

The main feature of low-temperature magnetization curves at $\mathbf{H} \parallel b$ is the presence of jump in magnetization corresponding to the spin-flop transition, detected by ESR. As shown at Fig. 11, the magnitude of the jump increases with cooling and its position shifts to lower fields. Jump in magnetization

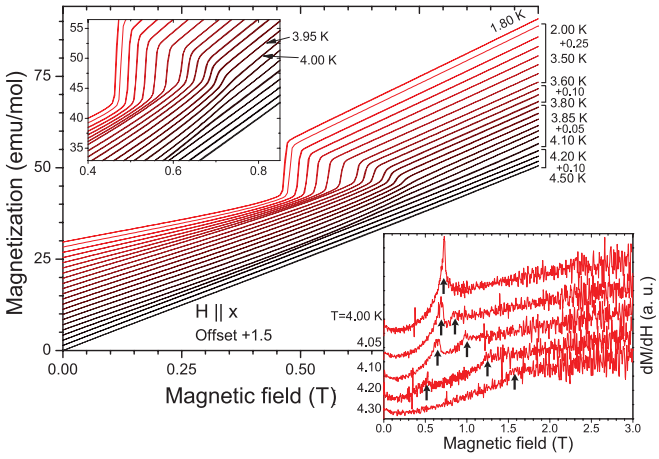

FIG. 11. (Color online) Isothermal low-field magnetization curves of the $Cu(pz)_2(ClO_4)_2$field along x. An offset of 1.5 emu/mol per curve is present. Upper inset: An expanded region around the temperature, where magnetization jump disappears. Lower inset: A few dM/dH curves are shown, allowing one to locate phase transitions between disordered and ordered phases, marked by arrows.

disappears around 4 ± 0.05 K, which is lower than T_N. The sharp increase in magnetization can also be seen in $M(T)$ curves, presented in Fig. 12. Crossing the spin-flop phase boundary by temperature in a constant field also gives a very pronounced step in magnetic moment. This step disappears at $\mu_0 H = 0.74$ T, and above this field, there appears a minimum on the M vs T dependence. Below the temperature of the minimum of the magnetization, there is a kink marking the onset of long-range order. The minimum and the kink are marked in Fig. 12. Both minimum and kink shift upwards in temperature with increasing field up to 9 T, though the former becomes less pronounced. Note that there is no offset in Fig. 12, and stacking of the curves reflects the nonlinearity of the magnetization process.

We derive the ordering point by a peak in the derivative $\partial(MT)/\partial T$, as suggested by Fisher.[11] We can also detect this transition by a peak in the derivative dM/dH of the isothermal

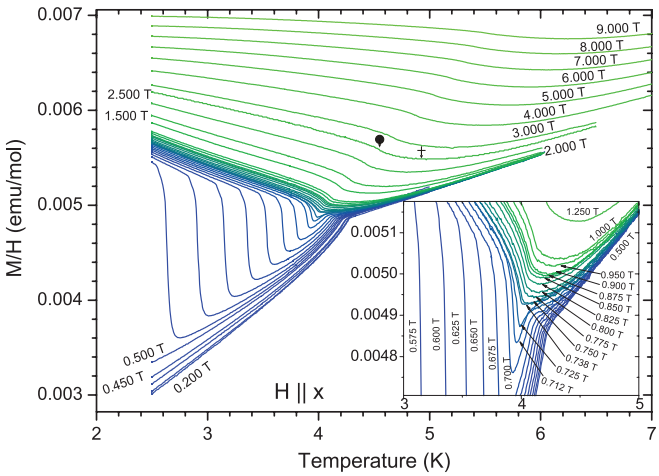

FIG. 12. (Color online) Normalized magnetization $M(T)/H$ for various magnetic fields, directed along x. Inset: An expanded region around the point, where magnetization jump vanishes.

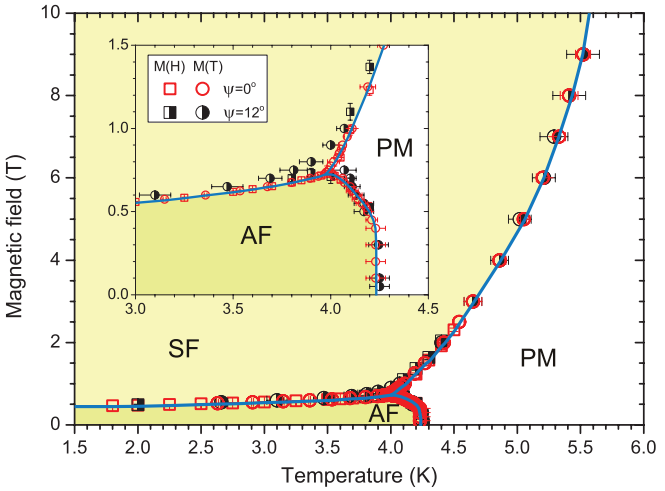

FIG. 13. (Color online) Phase diagram of the $Cu(pz)_2(ClO_4)_2$field along the easy axis. AF is the $\mathbf{l} \parallel x$ collinear antiferromagnetic phase, SF is the spin-flop antiferromagnetic phase, and PM is the paramagnetic phase. Circles are features in $M(T)$ curves, squares are features in $M(H)$, red points correspond to $\psi = 0°$ orientation, and black points correspond to $\psi = 12°$. Lines are a guide to the eye. In the inset, an expanded region around the bicritical point is shown.

magnetization curve, as displayed in the inset of Fig. 13. A final phase diagram, with points on phase boundaries obtained by both $M(T)$ and $M(H)$ scans, is presented in Fig. 13.

B. Field in *bc* plane

In Fig. 14, a collection of magnetization derivatives $dM(H)/dH$ for various directions of the magnetic field in the

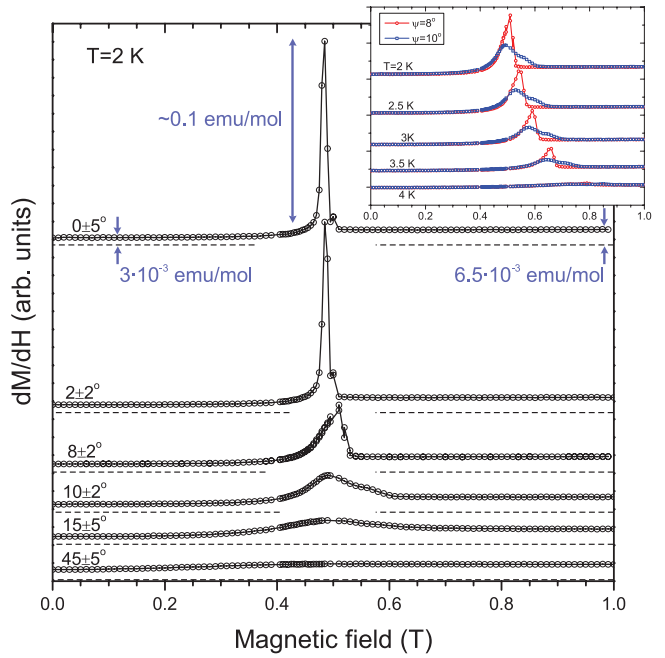

FIG. 14. (Color online) Magnetization derivative dM/dH for various directions of the magnetic field in the xy plane at $T = 2$ K. Dashed lines show zero for corresponding curves. Inset: Temperature dependencies of magnetization derivatives for directions $\psi = 8° \pm 2°$ and $\psi = 10° \pm 2°$.

xy plane is presented. $dM(H)/dH$ curves show a sharp peak at $\psi \to 0$, which broadens with misalignment. The left wing of the peak is always smooth, in contrast to a discontinuity in the right wing of the peak. The discontinuity exists up to a critical angle ψ_c, observed in angular dependences of ESR; see Figs. 4 and 5. When the tilt angle exceeds ψ_c, the dM/dH curve becomes completely smooth. The transition between smooth and discontinuous types of derivative, which affects mostly the right wing, occurs abruptly. This difference between the curves, corresponding to field tilts below and above ψ_c, is pronounced in a whole temperature range where spin-flop transition takes place, as shown in the inset of Fig. 14. The discontinuity of differential susceptibility dM/dH occurs exactly at the same magnitude of the magnetic field and in the same angular range $|\psi| < \psi_c$, as the anomalous ESR mode ν_a.

With further increase in ψ, the peak becomes less pronounced, and almost disappears when ψ approaches $\sim 45^\circ$. The magnetization curve at $\sim 45^\circ$ (this is the direction along natural crystal facets) does not show a step and demonstrates a smooth slope increase, as observed in Ref. 12.

We have also performed a study of a phase diagram with a magnetic field slightly tilted from the x axis. The orientation we chose was $\psi = 12 \pm 2^\circ > \psi_c$. Here, $Cu(pz)_2(ClO_4)_2$ still demonstrates an increase in magnetization near H_c, but the transition is regular, i.e., with a smooth derivative dM/dH on both sides of H_c. We locate H_c and T_N in the same way as was described before for $\mathbf{H} \parallel x$. The resulting phase boundaries are also shown in Fig. 13, and the difference between the phase diagram for exact and misaligned orientations along x is observed only near the bicritical point.

C. Field along middle and hard axes

The curves of normalized magnetization for the fields directed along middle axis y and hard axis z at Fig. 15 do not show spin flop, but demonstrate an increase of T_N in a magnetic field. The only qualitative difference between these two sets of curves is in the onset of the minimum of $M(T)$: for the field along y, the minimum appears for the applied fields between 1.5 and 2 T, while for the field along z, it is present even at $H \to 0$ (as independently confirmed by zero-field ac magnetization measurements).[12] Another feature of $M(T)$ curves at $\mathbf{H} \parallel y$ is the existence of an inflection point below T_N at low fields, in contrast to the case of $\mathbf{H} \parallel z$. As the field is increased, the inflection disappears.

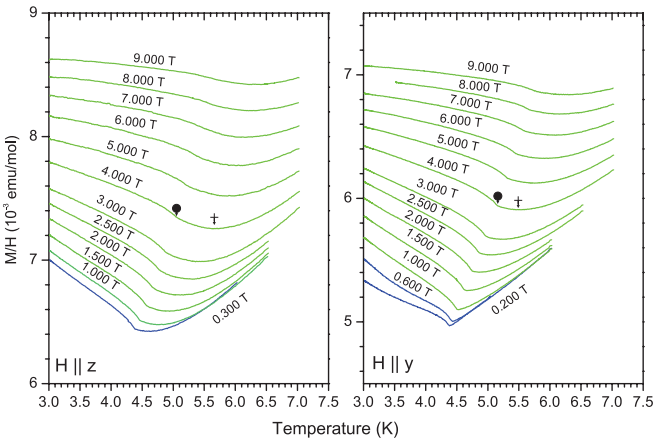

FIG. 15. (Color online) Normalized magnetization $M(T)/H$ for various magnetic fields, directed along z (left panel) and y (right panel). The kink and the minimum on the curves are marked by a droplet and a cross, respectively.

V. DISCUSSION

A. Biaxial model and spectra

In Sec. III, we have presented antiferromagnetic resonance (AFMR) spectra for various field directions. These spectra follow a biaxial collinear antiferromagnet paradigm for all magnetic field directions, except for a small solid angle corresponding to the anomalous mode. The anomalous mode is observed in a solid angle of about $10^{-2}4\pi$, close to the easy axis, and only above H_c. Resonance frequencies in this range of fields and angles correspond to a gapped branch (1) with $\Delta_a = 14$ GHz. This unexpected effect can be described as an in-plane anisotropy switching caused by spin flop, i.e., the resonant frequencies are that of a two-sublattice biaxial antiferromagnet, for which x turns abruptly from the easy into middle axis and y turns into the easy axis at the spin-flop point. This conclusion is made on the basis of the experimental observation of the anomalous mode, which appears at $H > H_c$ and has the frequency following the relation (A3), corresponding to middle-axis orientation of the field, instead of the expected (A7), derived for the easy-axis orientation.

We consider the magnetoelastic hypothesis, which might explain the switching of anisotropy at the spin-flop point. The in-plane anisotropy, marking the easy axis, originates from rhombic distortion of the square lattice; for $Cu(pz)_2(ClO_4)_2$, this distortion is due to a relative difference of $\sim 10^{-4}$ between the lattice constants b and c. In principle, the antiferromagnetic ordering may cause a striction of the same order of magnitude.[13] Because of the magnetostriction, the in-plane anisotropy may be dependent on the magnitude and the direction of sublattice magnetizations, and, therefore, it should change when the spin-flop transition takes place. One could expect the y axis to become the easy axis and x to become the middle axis immediately after the spin flop.

Nonetheless, a simple quantitative formulation of this approach, described in detail in Appendix B, does not capture a steplike angular dependence of the AFMR field in the xy plane, and is in contradiction to the observed relation between the zero-field gap and a critical field. The analysis of a complete Lagrangian, allowed by symmetry, should include several dozens of magnetoelastic and elastic terms and was not performed.

Another possibility, presumably explaining the nature of anomalous mode ν_a, is the existence of a phase other than collinear for $H > H_c, \psi < \psi_c$. This implies destabilization of the collinear phase by frustration when the external field compensates in-plane anisotropy. However, our measurements do not support this hypothesis: the magnetization curve $M(H)$ and phase boundary $T_N(H)$ are indistinguishable for $\psi < \psi_c$ and $\psi > \psi_c$ in fields above H_c.

The influence of a change of the direction and magnitude of zero-point fluctuations at the spin flop may also be of importance because anisotropic spin fluctuations also contribute to the energy of anisotropy.

Nevertheless, the nature of the anisotropy switching remains unclear.

To give a connection with the previous work (Ref. 7), we derive a relation between zero-field gaps $\Delta_{y,z}$ of antiferromagnetic resonance and the parameters of a microscopic model Hamiltonian. In the nearest-neighbor exchange approximation, the complete biaxial Hamiltonian reads as

$$\widehat{\mathcal{H}} = \sum_{\langle i,i'\rangle} J\widehat{\mathbf{S}}_i\widehat{\mathbf{S}}_{i'} - g\mu_B\mu_0 \sum_i \mathbf{H}\widehat{\mathbf{S}}_i - \sum_{\langle i,i'\rangle} \left(\delta J_y \widehat{S}_i^y \widehat{S}_{i'}^y + \delta J_z \widehat{S}_i^z \widehat{S}_{i'}^z\right), \quad (2)$$

where δJ_y and δJ_z are parameters of so-called exchange anisotropy. According to the linear spin-wave approximation, which have proven to be good for describing the k dependence of the spectrum in the vicinity of the Brillouin-zone center of $Cu(pz)_2(ClO_4)_2$ (Ref. 6), the energy gaps are related to exchange anisotropy parameters as

$$\Delta_{y,z} = 2\sqrt{2J\delta J_{y,z}}. \quad (3)$$

In this spin-wave approximation, the sublattice magnetization is supposed to be μ_B per magnetic ion, which is not the case of the $Cu(pz)_2(ClO_4)_2$, where a strong quantum reduction of about 50% is observed. A finer estimation for the case of $S = 1/2$ square-lattice antifferomagnet, considering $1/S$ corrections, was given by Weihong *et al.*:[14]

$$\Delta_{y,z} \simeq 1.2\sqrt{2J\delta J_{y,z}}. \quad (4)$$

Thus, this equation may be used for an estimation of $\delta J_{y,z}$. Spectroscopic gaps of 35 ± 2 and 11 ± 2 GHz are $\Delta_z = 1.68 \pm 0.1$ K and $\Delta_y = 0.53 \pm 0.1$ K, correspondingly. Hence, from Eq. (4) we extract $\delta J_z = 53.2$ mK and $\delta J_y = 5.3$ mK. This corresponds to relative exchange anisotropy $\delta J_z/J = 3.1 \times 10^{-3}$ and $\delta J_y/J = 3.1 \times 10^{-4}$. This is in agreement with previous neutron data, except for the parameter δJ_y, which was not resolved by the neutron-scattering experiment. We can characterize the observed anisotropy switching in terms of changing of parameters of Hamiltonian (2). It corresponds to transformation of δJ_y into δJ_y^*, which is of *negative* sign and equals -6.7 mK.

B. Phase diagrams

Phase diagrams for the x, y, and z directions of the magnetic field are presented in Fig. 16. For the y and z directions, the phase diagrams are analogous, with a monotonous increase of T_N. For the field along x, the phase diagram is more complicated, with a bicritical point, where spin-flop, ordered and paramagnetic phases meet. The phase diagram presents the spin-flop transition and the bicritical point in addition to the phase boundaries reported in the previous work using neutron-scattering and specific-heat measurements.[6]

The field at which the antiferromagnetic resonance mode ν_3 is observed also marks the spin-flop transition (see the Appendix). From the ESR experiment, we get $\mu_0 H_c^{\mathrm{ESR}} =$ 0.45 T at $T = 1.3$ K (see Fig. 9); this field increases with temperature. The temperature dependence of H_c derived from ESR is consistent with the magnetization measurements, as shown in Fig. 16.

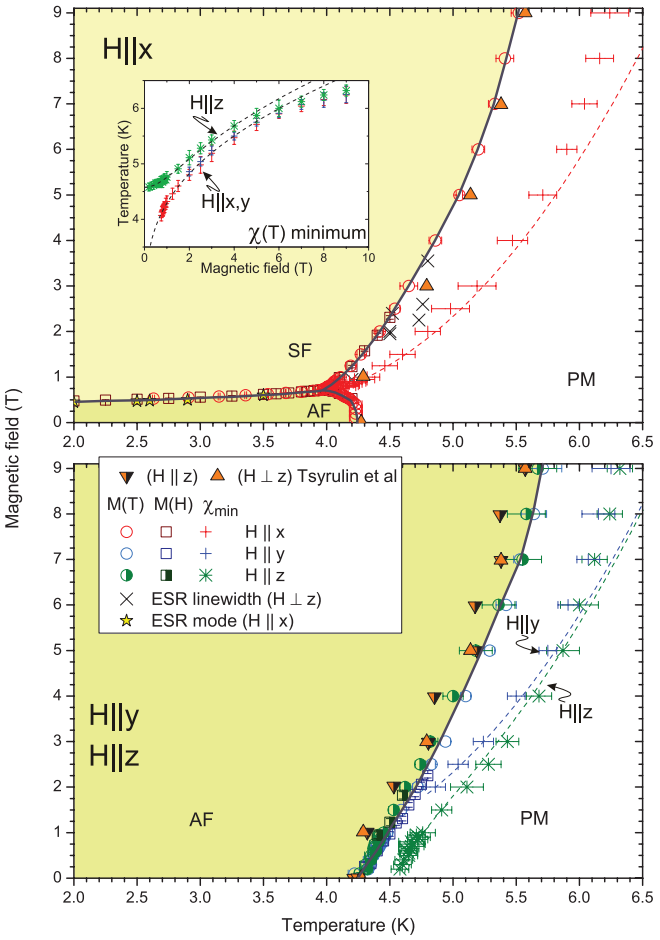

FIG. 16. (Color online) Phase diagrams for $H \parallel x$ (upper panel) and $H \parallel yz$ (lower panel) directions. Points are experimental data: circles for $M(T)$ and squares for $M(H)$ features. Stars and diagonal crosses mark phase transitions determined by ESR; solid triangles are data from Ref. 6. Horizontal crosses (x, y) and snowflakes (z) are minima in $M(T)$. Solid lines are a guide to the eye; dashed lines are fit (5) for $T_{\mathrm{min}}(H)$. The fit for all three orientations is separately shown in the inset in the upper panel.

The minima of $M(T)$ are also plotted, showing different behavior for all three directions. While for $\mathbf{H} \parallel z$ the minimum persists up to the $H = 0$ limit, for different directions it appears only at some finite field at which T_{min} reaches T_N.

The reason for this minimum may be qualitatively explained by the following consideration: for an easy-plane antiferromagnet, it is natural to have an anisotropic susceptibility, which is larger for the out-of-plane direction. In the case of a 2D antiferromagnet with $\delta J_z \ll J$, one should expect this anisotropic behavior to rise only at low temperatures, when $T < J$. Numerical simulations of HSLAF with a weak easy-plane anisotropy[8] show that the tendency for an increase of magnetization at $\mathbf{H}\|\mathbf{z}$ due to the onset of planar correlations overcomes the tendency for its decrease due to short-range AF order. Thus a characteristic minimum in $\chi(T)$ marks a crossover from Heisenberg to XY behavior. Cuccolli *et al.*,[8]

using a QMC data analysis, suggested a formula for the estimation of $T_{\min}$ in a case of easy-plane HSLAF model,

$$T_{\min} = \frac{4\pi\rho_s}{\ln\left(\frac{C}{\delta_{\text{eff}}}\right)}. \tag{5}$$

Here, $\rho_s \simeq 0.22J$ is the renormalized spin stiffness, δ_{eff} is the relative anisotropy, and $C \simeq 160$ is the dimensionless constant. It has also been found that the presence of an external magnetic field in 2D magnets makes them effectively easy plane and induces both a Berezinsky-Kosterlitz-Thouless transition at finite temperature and a minimum in $\chi(T)$ above it (Ref. 15). In the absence of long-range order, when a *local* order parameter $\mathbf{l}$ is formed, the orientation $\mathbf{l} \perp \mathbf{H}$ provides an energy gain. Hence, the short-range order parameter becomes 2D instead of 3D in the isotropic case and the effective anisotropy energy in this field-induced XY behavior is proportional to H^2.

For the orientation of the magnetic field $\mathbf{H} \perp z$ for a strong enough field ($g\mu_B\mu_0 H \gtrsim \sqrt{\delta J_z J}$), we consider "effective" easy-plane anisotropy induced by an external field. The easy plane of this anisotropy is perpendicular to the field. We take this anisotropy in the form derived in Ref. 15 for HSLAFM,

$$\delta_{\text{eff}}^{xy} = \beta\left(\frac{g_{xy}\mu_B\mu_0 H}{k_B J}\right)^2, \tag{6}$$

where β is a dimensionless parameter. Here we disregard smaller anisotropy δJ_y, as the experimental $T_{\min}(H)$ in the x and y directions is the same within the error bars.

For the case $\mathbf{H} \parallel z$, the easy-plane anisotropy originates due to the combination of the natural and field-induced anisotropy. We empirically combine these two factors which were analyzed separately in QMC simulations,[15,16]

$$\delta_{\text{eff}}^{z} = \frac{\delta J_z}{J} + \beta\left(\frac{g_z\mu_B\mu_0 H}{k_B J}\right)^2. \tag{7}$$

Fitting experimental data for $T_{\min}$ with Eq. (5), where δ_{eff} is set as δ_{eff}^{xy} or δ_{eff}^{z}, and parameters $J = 18.1$ K and $C = 160$ are fixed, we yield $\rho_s \simeq 0.24J$, $\delta J_z \simeq 0.023$ K, and $\beta \simeq 0.1$, which is quite close to the result of Cucolli *et al.* (Ref. 15). Fits are shown in Fig. 16 with dashed lines. This result can be considered as another indication of the 2D correlations developing in $Cu(pz)_2(ClO_4)_2$ at $T > T_N$. Nonetheless, the value of δJ_z obtained by this fit is in better agreement with the estimation by Eq. (3), which does not take into account quantum renormalization of the gap, than with Eq. (4), which considers $1/S$ corrections.

For $\mathbf{H} \parallel x$ (i.e., the field along the easy axis), there is a bicritical point (H_c, T_c). Three phase transition lines meet in this point: second-order paramagnetic to collinear antiferromagnetic phase transition (PM-AF), second-order paramagnetic to flopped antiferromagnetic phase transition (PM-SF), and first-order spin-flop phase transition (AF-SF). In the vicinity of the bicritical point, the following scaling equations are expected:[17] for AF-SF, the transition temperature dependence for the critical field is

$$H^2(T) - H_c^2 = A\left(\frac{T}{T_c} - 1\right), \tag{8}$$

while for ordering transitions to AF and SF phases relations between the magnetic field and ordering, temperatures are

$$H^2(T) - H_c^2 = A\left(\frac{T}{T_c} - 1\right) - B_{AF}\left(\frac{T}{T_c} - 1\right)^{\phi} \tag{9}$$

and

$$H^2(T) - H_c^2 = A\left(\frac{T}{T_c} - 1\right) + B_{SF}\left(\frac{T}{T_c} - 1\right)^{\phi}, \tag{10}$$

correspondingly. For a "classical" 3D antiferromagnet, the scaling exponent is known to be $\phi = 1.25$ for uniaxial and $\phi = 1.175$ for biaxial anisotropy. Theory also suggests an amplitude ratio $Q = B_{SF}/B_{AF} = 1$ for the former case.[17,18] In contrast, for the pure 2D case with easy-axis anisotropy, the bicritical point is expected[19–21] to occur only at $T = 0$; a simple argument for that is the following: when easy-axis anisotropy is compensated by the external field, the system becomes equivalent to a nonperturbed two-dimensional Heisenberg model, which can possess long-range order only at zero temperature. The PM-AF and PM-SF phase boundaries, which meet at $T = 0$, are defined by

$$\left|H^2(T) - H_c^2\right| \propto T^{-2}\exp\left(-\frac{4\pi\rho_s}{T}\right). \tag{11}$$

The above equation is valid only in the absence of additional anisotropies and interlayer couplings, while in the case of $Cu(pz)_2(ClO_4)_2$, both of these perturbations are present and the bicritical point is at $T > 0$. A numerical proof for the latter statement can be found, e.g., in the Monte Carlo study of the classical anisotropic XY antiferromagnet on a square lattice (Ref. 22), where the phase diagram strongly resembles that of a 3D easy-axis AFM. Hence, the phase diagram of $Cu(pz)_2(ClO_4)_2$ turns out to be an intermediate case between ideal 2D and conventional 3D anisotropic antiferromagnets. A straightforward fit of the experimental data with Eqs. (8)–(10) gives the bicritical point at $T_c = 3.97$ K, $\mu_0 H_c = 0.73$ T with scaling exponent $\phi = 1.4$ and amplitude ratio $Q = 1.78$. Fixing the value of ϕ to the theoretically suggested value for a 3D antiferromagnet, $\phi_{3D} = 1.175$, leads to $T_c = 3.99$ K, $\mu_0 H_c = 0.738$ T, and $Q = 1.54$, but with a worse fit quality. The data and fits are presented in Fig. 17, together with the numerical quality criterion—the sum of the average least squares for all three formulas (8)–(10). It can be concluded that a reliable estimation of the universal parameters from our data is $\phi = 1.4 \pm 0.2$ and $Q = 1.8 \pm 0.2$, and the bicritical point is located at $\mu_0 H_c = 0.730 \pm 0.006$ T and $T_c = 3.97 \pm 0.03$ K. The region $\Delta T \simeq 0.2$ K where the scaling equations are fulfilled is about 5% of T_c, which is significantly larger than for the classical three-dimensional uniaxial antiferromagnet MnF_2 [$\Delta T/T_c \sim 10^{-3}$ (Ref. 18)], though smaller than for the quasi-2D compound Rb_2MnF_4 [$\Delta T/T_c \sim 0.26$ (Ref. 21)], with a purely uniaxial anisotropy. These facts, as well as the larger value of critical index $\phi = 1.4 > \phi_{3D}$, result in the conclusion that $Cu(pz)_2(ClO_4)_2$ presents an intermediate behavior between 3D and 2D models in the vicinity of the bicritical point.

The observed dependence of the phase diagram in the bicritical point range on the field orientation is natural because the bicritical point is very sensitive to field misalignment.[18]

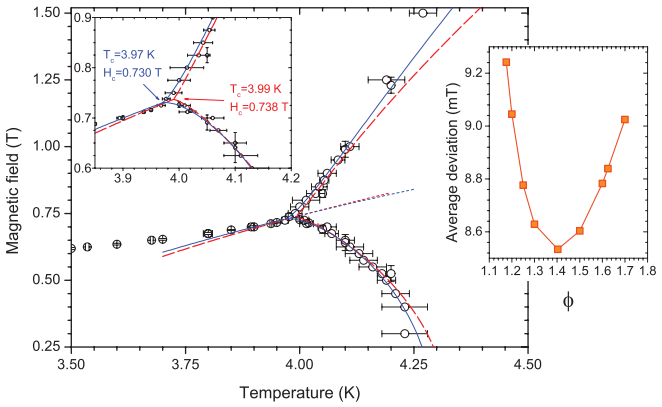

FIG. 17. (Color online) Scaling in the vicinity of the bicritical point. Blue solid and red dashed lines are fits [(8)–(10)] with $\phi = 1.4$ and $\phi = 1.175$ correspondingly; dotted lines are extension of Eq. (8) to the $T > T_c$ region. Left inset: Magnified part of main plot. Right inset: Fit deviation (see text) vs critical exponent ϕ.

On the contrary, away from the region around H_c, the phase boundaries for $\psi = 0^\circ$ and $\psi = 12^\circ$ coincide within error bars.

VI. CONCLUSIONS

In the present work, we have studied the AFMR spectra and magnetization curves of HSLAFM $Cu(pz)_2(ClO_4)_2$. These measurements reveal the presence of biaxial anisotropy in $Cu(pz)_2(ClO_4)_2$instead of the easy-plane formulation used earlier. From the ESR experiments, we have derived two energy gaps, $\Delta_z \simeq 35$ and $\Delta_y \simeq 11$ GHz. The weak in-plane anisotropy is responsible for the spin-flop phase transition at $\mu_0 H_c \simeq 0.4$ T in the $\mathbf{H} \parallel x$ direction. The AFMR spectra also show that weak in-plane anisotropy is changing its sign at the spin-flop transition. This anisotropy reversal, occurring in a manner of switching, may be also observed as a phase transition at changing the orientation of the magnetic field within the bc plane, at the critical angle 10 ° with respect to the easy-axis direction. The conjecture that this anomaly might be of magnetoelastic origin may, by simplified treatment, explain the anisotropy reversal at the spin flop, but is not consistent with the steplike angular dependence of the ESR field or frequency. It is also not consistent with the observed relation between the energy gap Δ_y and spin-flop field H_c. The nature of the abrupt reversal of the weak anisotropy remains unclear.

The hypothesis which is probably worthwhile to analyze theoretically is a possible change of the direction and magnitude of zero-point spin fluctuations at the spin flop. A change of the contribution of fluctuations to the energy of the anisotropy may also change the effective anisotropy of the ordered spin component.

The field dependence of the temperature of the minimum on $M(T)$ curves for three principal orientations is found to be in agreement with the results of the numerical simulation of HSLAFM.[8] The increase of T_N in the external field has been found for all orientations, in agreement with previous measurements. The scaling exponent $\phi = 1.4 \pm 0.2$ of the phase boundaries near the bicritical point is intermediate between the 2D and 3D models.

Accounting for the observed weak anisotropy might be significant for the correct estimation of other weak interactions, e.g., next-nearest-neighbor and interlayer exchange from experimental data.[23] Similar anisotropy can be present in another HSLAFM of the Cu-pz family [namely, $Cu(pz)_2(BF_4)_2$ and $[Cu(pz)_2(NO_3)](PF_6)$], as according to Xiao's magnetization data[12] there are signatures of spin-flop transitions as well.

We note that for deuterated $Cu(pz)_2(ClO_4)_2$, the difference between b and c, resulting in the weak anisotropy, is larger than for a regular sample with hydrogen, so it would be of interest to test if the in-plane anisotropy is the same in a deuterated sample. Other possible future experiments include NMR and neutron scattering with the field along x to probe the magnetic structure as well as search for anomaly in magnetic field dependencies of low-temperature elastic properties (magnetostriction, ultrasound propagation, etc.).

ACKNOWLEDGMENTS

The authors would like to thank O. S. Volkova and A. N. Vasiliev (Moscow State University) and A. Zheludev (ETH Zürich) for the opportunity to use their experimental facilities and assistance with it. Also special thanks to V. N. Glazkov, L. E. Svistov, S. S. Sosin, V. I. Marchenko, M. E. Zhitomirsky, and W. E. A. Lorenz for fruitful and stimulating discussions. This work was supported by RFBR Grant No. 12-02-00557.

APPENDIX A: AFMR FREQUENCIES OF A BIAXIAL ANTIFERROMAGNET

A theory for AFMR in a two-sublattice antiferromagnet with biaxial anisotropy was developed in the 1950s.[10] For both orientations of the magnetic field along the hard and middle axis (z and y) in the ground state, we have the antiferromagnetic order parameter $\mathbf{l} \parallel x$, and this orientation of $\mathbf{l}$ is independent of the external field magnitude.

Magnetic resonance frequencies for $\mathbf{H} \parallel z$ are

$$\nu_{zz} = \sqrt{\left(\frac{g_z \mu_B}{2\pi\hbar}\mu_0 H\right)^2 + \Delta_z^2}, \tag{A1}$$

$$\nu_{zy} = \Delta_y; \tag{A2}$$

and for $\mathbf{H} \parallel y$, we have

$$\nu_{yy} = \sqrt{\left(\frac{g_y \mu_B}{2\pi\hbar}\mu_0 H\right)^2 + \Delta_y^2}, \tag{A3}$$

$$\nu_{yz} = \Delta_z. \tag{A4}$$

At the orientation of the magnetic field along the easy axis, the case is more complicated, as the ground state is field dependent. There is a spin-flop transition with an abrupt change from $\mathbf{l} \parallel x$ to $\mathbf{l} \parallel y$. The critical field of this transition is

$$\mu_0 H_c = 2\pi \frac{\hbar \Delta_y}{g_x \mu_B}. \tag{A5}$$

This transition is accompanied by a jump in magnetization. The ESR frequencies below and above H_c are the following:

For $H < H_c$,

$$\nu_{1,2} = \sqrt{\left(\frac{g_x\mu_B}{2\pi\hbar}\mu_0 H\right)^2 + \frac{\Delta_y^2+\Delta_z^2}{2} \mp \sqrt{2\left(\frac{g_x\mu_B}{2\pi\hbar}\mu_0 H\right)^2\left(\Delta_y^2+\Delta_z^2\right) + \left(\frac{\Delta_y^2-\Delta_z^2}{2}\right)^2}}. \quad \text{(A6)}$$

For $H > H_c$,

$$\nu_4 = \sqrt{\left(\frac{g_x\mu_B}{2\pi\hbar}\mu_0 H\right)^2 - \Delta_y^2}, \quad \text{(A7)}$$

$$\nu_5 = \sqrt{\Delta_z^2 - \Delta_y^2}. \quad \text{(A8)}$$

The resonant mode ν_3 with the vertical $\nu_3(H)$ dependence corresponds to a spin-flop transition, as the system is allowed to absorb energy in a band of frequencies in the critical point. Modes ν_1 and ν_4 are softened at the critical field H_c. For the intermediate-field orientations, we calculated the frequencies of spin resonance numerically within the same formalism.

APPENDIX B : MAGNETOELASTIC CORRECTION

For a description of the ESR modes at $T \to 0$, we use macroscopic exchange symmetry formalism.[24] This formalism, in particular, reproduces the results of a mean-field theory of a two-sublattice antiferromagnet with biaxial anisotropy.[10] In the framework of the exchange approach, the spin structure is considered to be collinear, and the anisotropy of a relativistic origin, and magnetization, induced by the external field, are taken as perturbations. Though being applicable only in fields $H \ll H_{\rm sat}$, this formalism is model independent and allows easy introduction of additional anisotropy terms. As the saturation field in $Cu(pz)_2(ClO_4)_2$ constitutes almost 50 T, restriction on the field magnitude is not an issue for the exchange symmetry formalism applicability. Our calculations are based on the following Lagrange function per mole of the compound (in the Gaussian unit system):

$$\mathcal{L} = \frac{\chi_\perp}{2\gamma^2}(\dot{\mathbf{l}} + \gamma[\mathbf{H}\times\mathbf{l}])^2 - U_a. \quad \text{(B1)}$$

Here, $\gamma = \frac{g\mu_B}{\hbar}$ is the gyromagnetic ratio; unit vector $\mathbf{l}$ with the orientation, given by angles φ and θ shown in Fig. 4, is the order parameter; $\mathbf{H}$ is the magnetic field; and $\chi_\perp$ is the magnetic susceptibility in the direction perpendicular to $\mathbf{l}$. Equation (B1) also implies $\chi_\parallel = 0$ at zero temperature. The term $U_a = \eta l_y^2 + \zeta l_z^2$ is the anisotropy energy. We assume positive constants η and ζ, $\eta < \zeta$. Hence, $\mathbf{l} \parallel x$ minimizes anisotropy energy.

The ground-state and magnetic-resonance frequencies may be calculated using this Lagrange function, as described in Ref. 24. The ground state and the spectrum are identical to that of Ref. 10, described above. The anisotropy constants may be expressed via energy gaps, $\eta = \chi_\perp(2\pi\Delta_y^2)/2\gamma^2$ and $\zeta = \chi_\perp(2\pi\Delta^2)_z/2\gamma^2$, where $\Delta_z > \Delta_y$ are the energy gaps which one actually observes in the ESR experiment. With this substitution, the Lagrange function (B1) is

$$\mathcal{L} = \frac{\chi_\perp}{\gamma^2}\left\{\frac{1}{2}(\dot{\mathbf{l}} + \gamma[\mathbf{H}\times\mathbf{l}])^2 - \frac{(2\pi\Delta_z)^2}{2}l_z^2 - \frac{(2\pi\Delta_y)^2}{2}l_y^2\right\}, \quad \text{(B2)}$$

and the corresponding potential energy in the nonzero magnetic field is

$$\mathcal{E} = \frac{\chi_\perp}{\gamma^2}\left\{-\frac{\gamma^2}{2}[\mathbf{H}\times\mathbf{l}]^2 + \frac{(2\pi\Delta_z)^2}{2}l_z^2 + \frac{(2\pi\Delta_y)^2}{2}l_y^2\right\}. \quad \text{(B3)}$$

Monoclinic symmetry allows for another second-order term, $l_y l_z$. Such a term results in a tilt of hard and middle anisotropy axes, leaving the easy axis undisturbed. In our experimental data, related to xz-plane rotation of the magnetic field (Fig. 7), we do not notice any significant tilt of the middle axis from the c direction, and, therefore, we do not take the $l_y l_z$ term into account.

We have to note that the anisotropic term ηl_y^2 originates from a weak orthorhombic distortion of a square lattice. Due to this distortion, the lattice constants b and c differ in a relative sense for $\sim 10^{-4}$. Hence, this term should be small in comparison with, e.g., ζl_z^2, and can be comparable with the contributions of a higher order in components of $\mathbf{l}$. There is a term $B(l_x l_y)^2$ among the fourth-order terms, allowed by symmetry for $Cu(pz)_2(ClO_4)_2$. This term couples the components l_x,l_y and could result in the "anisotropy reversal" as a result of $\mathbf{l}$ reorientation. Indeed, considering a modified Lagrange function

$$\mathcal{L} = \frac{\chi_\perp}{\gamma^2}\left\{\frac{1}{2}(\dot{\mathbf{l}} + \gamma[\mathbf{H}\times\mathbf{l}])^2 - \frac{(2\pi\Delta_z)^2}{2}l_z^2 - \frac{(2\pi\Delta_y)^2}{2}l_y^2\right\} + B(l_x l_y)^2, \quad \text{(B4)}$$

we obtain approximate frequencies, corresponding to in-plane fluctuations of $\mathbf{l}$, for ground states before and after reorientation:

$$\tilde{\nu}(l \parallel x) = \sqrt{\Delta_y^2 + \frac{2B}{\chi_\perp}\left(\frac{g_x\mu_B}{2\pi\hbar}\right)^2 - \left(\frac{g_x\mu_B}{2\pi\hbar}H\right)^2},$$

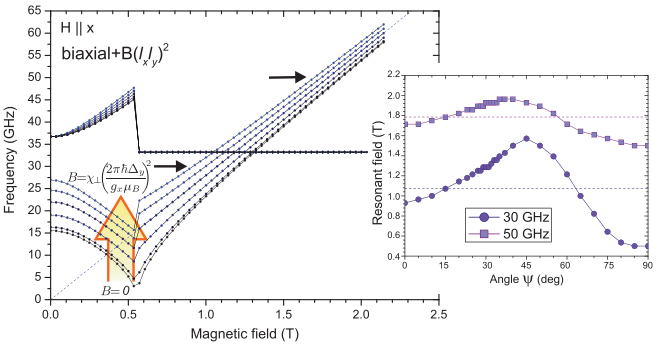

FIG. 18. (Color online) Spectra of model (B4) for various values of the quartic term. The field is directed along x. Arrows mark frequencies at which angular dependencies for $B = \chi_\perp(\frac{2\pi\hbar\Delta_y}{g_x\mu_B})^2$ are shown in the inset; dashed lines are the expectation for paramagnetic resonance.

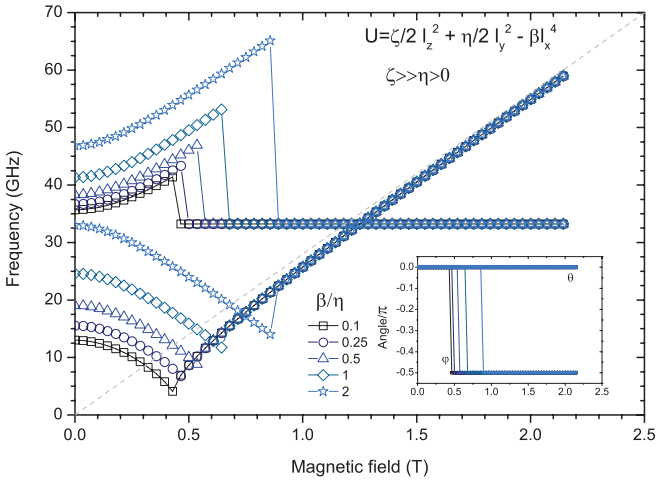

FIG. 19. (Color online) Spectra of the model with a quartic term $-\beta l_x^4$, $\mathbf{H} \parallel x$. Dashed line is paramagnetic resonance.

and

$$\tilde{\nu}(l \parallel y) = \sqrt{-\Delta_y^2 + \frac{2B}{\chi_\perp}\left(\frac{g_x \mu_B}{2\pi\hbar}\right)^2 + \left(\frac{g_x \mu_B}{2\pi\hbar} H\right)^2}.$$

The field-independent constants under the square-root signs in these relations may be treated by use of model (B2) and relations (A6) and (A7) as the anisotropy constant for in-plane anisotropy (note that these constants should be taken with the opposite signs). Thus, if $B > 0$ is large enough, the in-plane anisotropy effectively changes its sign. A significant value of B might be provided by a magnetoelastic interaction. There are 13 elastic terms of the form of $u_{ik}u_{mn}$ and 20 magnetoelastic terms of the form of $u_{ik}l_m l_n$ allowed by symmetry for $Cu(pz)_2(ClO_4)_2$ (Ref. 25). From these terms, we take for the magnetoelastic contribution to potential energy (B3) the following terms:

$$E_{me} \propto u_{xy} l_x l_y, \tag{B5}$$

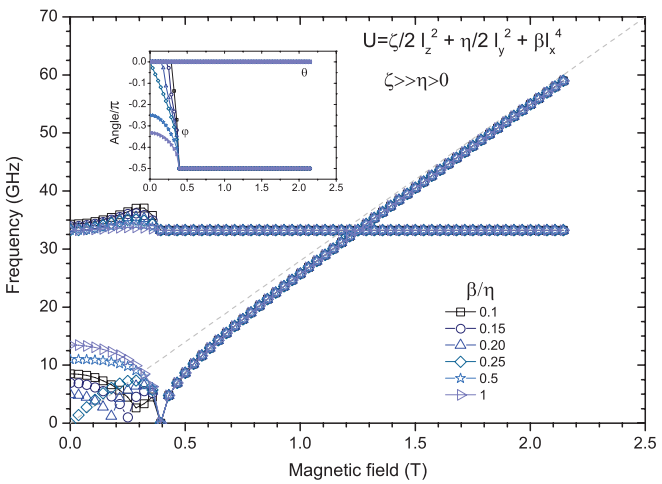

FIG. 20. (Color online) Spectra of the model with a quartic term βl_x^4, $\mathbf{H} \parallel x$. Dashed line is paramagnetic resonance.

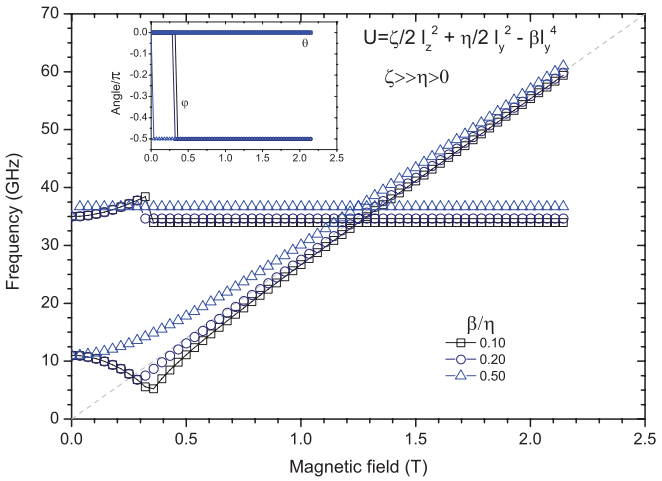

FIG. 21. (Color online) Spectra of the model with a quartic term $-\beta l_y^4$, $\mathbf{H} \parallel x$. Dashed line is paramagnetic resonance.

and

$$E_{ee} \propto \frac{u_{xy}^2}{2}. \tag{B6}$$

These terms couple l_x and l_y. Here, u_{ik} are components of the strain tensor.

Minimization of energy, including the above-described magnetoelastic correction (B5) and (B6), with respect to strain variable u_{xy}, will result in the magnetoelastic correction in the form of $Bl_x^2 l_y^2$.

We numerically calculate the ground state and spectrum of the model (B4). For our numerical work, we choose parameters $\Delta_z = 37$ and $\Delta_y = 15$ GHz, and follow the perturbations introduced by the quartic term $Bl_x^2 l_y^2$. In Fig. 18, numerically calculated spectra for the field along x and different values of B [namely, $\frac{2B}{\chi_\perp}(\frac{g_x \mu_B}{2\pi\hbar\Delta_y})^2 = 0,0.1,0.5,1,1.5,2$] are presented. Indeed, we can choose the value of B, which is large enough to push mode ν_4 above paramagnetic resonance, as clearly seen in Fig. 18. But there remains a crucial difference between the properties of model (B4) and the experimental data

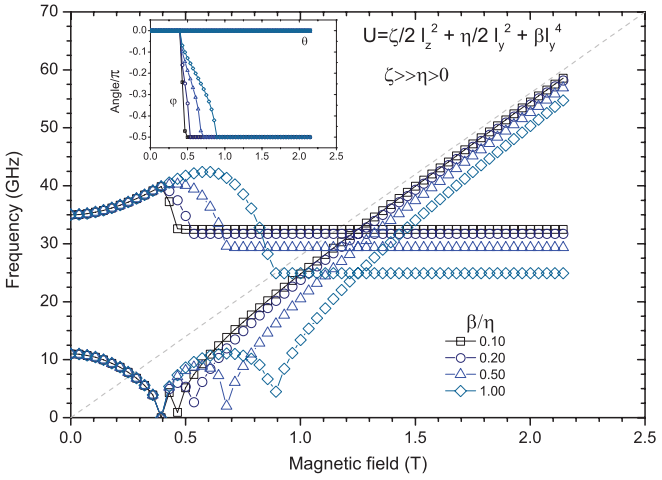

FIG. 22. (Color online) Spectra of the model with a quartic term βl_y^4, $\mathbf{H} \parallel x$. Dashed line is paramagnetic resonance.

because the angular dependence is not described. We found from the ESR experiment that the angular dependence of the resonance line shows a step when switching from ν_a to ν_4; the anomalous mode ν_a exists in a narrow angle range near the x axis, and outside of this range all the data are perfectly described by a simple biaxial model. In contrast, the model with the strong B term (B4) shows smooth angular dependence (see inset in Fig. 18), which differs significantly from both the simple biaxial model (B2) and experimental data (as in Fig. 5). Furthermore, as seen from Fig. 18, enhancement of the B term also increases a lower zero-field gap, while the critical field of the spin-flop transition is still determined by Δ_y^2 alone, as the $l_x^2 l_y^2$ combination gives the same contribution to energies of both the $\mathbf{l} \parallel x$ and $\mathbf{l} \parallel y$ phases. Therefore, the magnetoelastic approach (B4) predicts the transposition of the antiferromagnetic resonance frequency above the value of the paramagnetic resonance frequency, which is one of the manifestations of the reversal of the in-plane anisotropy. Nevertheless, at the same time, the angular dependence of the resonance field and relation between the gap and critical field do not correspond to the experiment even qualitatively.

Other related quartic terms also could not describe the observed anomaly. We have analyzed in the same way the influence of anisotropic terms $\pm\beta l_x^4$ and $\pm\beta l_y^4$. The results of the calculation of the ground states (equilibrium values of φ,θ) and frequency-field dependencies are given in Figs. 19–22. One can see that it is impossible to find a value of β which would correspond to the observed pulling of the frequency above the paramagnetic resonance frequency for $H > H_c$ along with the softening of the mode at $H < H_c$, and with the valid relation $\gamma H_c = \Delta_y$.

[1] E. Manousakis, Rev. Mod. Phys. **63**, 1 (1991).
[2] S. R. White and A. L. Chernyshev, Phys. Rev. Lett. **99**, 127004 (2007).
[3] F. M. Woodward, P. J. Gibson, G. B. Jameson, C. P. Landee, M. M. Turnbull, and R. D. Willett, Inorg. Chem. **49**, 4256 (2007).
[4] C. Yasuda, S. Todo, K. Hukushima, F. Alet, M. Keller, M. Troyer, and H. Takayama, Phys. Rev. Lett. **94**, 217201 (2005).
[5] T. Lancaster, S. J. Blundell, M. L. Brooks, P. J. Baker, F. L. Pratt, J. L. Manson, M. M. Conner, F. Xiao, C. P. Landee, F. A. Chaves, S. Soriano, M. A. Novak, T. P. Papageorgiou, A. D. Bianchi, T. Herrmannsdörfer, J. Wosnitza, and J. A. Schlueter, Phys. Rev. B **75**, 094421 (2007).
[6] N. Tsyrulin, F. Xiao, A. Schneidewind, P. Link, H. M. Rønnow, J. Gavilano, C. P. Landee, M. M. Turnbull, and M. Kenzelmann, Phys. Rev. B **81**, 134409 (2010).
[7] N. Tsyrulin, T. Pardini, R. R. P. Singh, F. Xiao, P. Link, A. Schneidewind, A. Hiess, C. P. Landee, M. M. Turnbull, and M. Kenzelmann, Phys. Rev. Lett. **102**, 197201 (2009).
[8] A. Cuccoli, T. Roscilde, R. Vaia, and P. Verrucchi, Phys. Rev. Lett. **90**, 167205 (2003).
[9] C. Poole, *Electron Spin Resonance: A Comprehensive Treatise on Experimental Techniques* (Dover, New York, 1983).
[10] T. Nagamiya, K. Yosida, and R. Kubo, Adv. Phys. **4**, 1 (1955).
[11] M. E. Fisher, Philos. Mag. **7**, 1731 (1962).
[12] F. Xiao, F. M. Woodward, C. P. Landee, M. M. Turnbull, C. Mielke, N. Harrison, T. Lancaster, S. J. Blundell, P. J. Baker, P. Babkevich, and F. L. Pratt, Phys. Rev. B **79**, 134412 (2009).
[13] B. Morosin, Phys. Rev. B **1**, 236 (1970).
[14] Zheng Weihong, J. Oitmaa, and C. J. Hamer, Phys. Rev. B **43**, 8321 (1991).
[15] A. Cuccoli, T. Roscilde, R. Vaia, and P. Verrucchi, Phys. Rev. B **68**, 060402 (2003).
[16] A. Cuccoli, T. Roscilde, V. Tognetti, R. Vaia, and P. Verrucchi, Phys. Rev. B **67**, 104414 (2003).
[17] J. M. Kosterlitz, D. R. Nelson, and M. E. Fisher, Phys. Rev. B **13**, 412 (1976).
[18] A. R. King and H. Rohrer, Phys. Rev. B **19**, 5864 (1979).
[19] D. R. Nelson and R. A. Pelcovits, Phys. Rev. B **16**, 2191 (1977).
[20] J. M. Kosterlitz and M. A. Santos, J. Phys. C **11**, 2835 (1978).
[21] R. Cowley, A. Aharony, R. Birgeneau, R. Pelcovits, G. Shirane, and T. Thurston, Z. Phys. B **93**, 5 (1993).
[22] M. Holtschneider and W. Selke, Phys. Rev. B **76**, 220405 (2007).
[23] M. Siahatgar, B. Schmidt, and P. Thalmeier, Phys. Rev. B **84**, 064431 (2011).
[24] A. F. Andreev and V. I. Marchenko, Sov. Phys. Usp. **23**, 21 (1980).
[25] M. Lines, Phys. Rep. **55**, 133 (1979).